JOURNAL OF MATERIALS SCIENCE 37 (2002) 845–853

Nanoindentation investigation of micro-fracture wear mechanisms in polycrystalline alumina

P. C. TWIGG*, F. L. RILEY
Department of Materials, School of Process Environmental and Materials Engineering, University of Leeds, Leeds LS2 9JT, UK

S. G. ROBERTS
Department of Materials, University of Oxford, Parks Road, Oxford OX1 3PH, UK

The initiation of surface damage under point loading has been investigated in polycrystalline alumina materials using low load continuous depth-sensing indentation equipment (nanoindentation). Pure alumina and liquid phase sintered materials containing 10% by weight of magnesium or calcium monosilicate have been examined and data obtained from plots of displacement as a function of load assessed in relation to erosive wear rates. In the pure alumina material, discontinuities ("pop-ins") in the load-displacement trace appear to be associated with the induction of radial cracking around a plastic impression. The pop-ins provide information on the indentation load at which fracture was initiated, and an estimate of the energy associated with crack formation. SEM imaging of the indentations before and after etching allowed crack paths to be related to microstructural features. © *2002 Kluwer Academic Publishers*

1. Introduction

The wear of a brittle polycrystalline ceramic can occur by several mechanisms, the relative importance of which depends in part on the wear conditions. In general, high applied loads or high rates of energy input lead to severe surface damage, while milder wear conditions lead to polishing. Severe wear damage, causing surface roughening, is generally attributable to the removal of material by mechanisms involving an accumulation of micro-fracture events at individual grains. The slower wear mechanism, which often results in surface polishing, has been attributed to plastic and tribochemical processes [1, 2]. To minimize the wear rate of a given material, wear conditions ideally should be controlled so as to reduce the extent of mechanical wear damage. In practice this is difficult to achieve because materials are normally used close to their limits, and microfracture mechanisms thus tend to dominate the wear process. Material composition and microstructure are important additional, and usually interlinked, factors controlling the boundry between the two wear regimes and thus the wear rate.

Polycrystalline aluminas obtained by liquid phase sintering micrometre powders are the most widely used of the technical ceramics for applications where good resistance to wear is required. Typical liquid phase sintering additive systems consist of metal silicates such as those of magnesium and calcium, either singly, or in combination, and often in conjunction with other oxides such as titanium dioxide or zirconium dioxide [3]. Understanding of the factors controlling microfracture in these materials, and of the conditions favouring the onset of microfracture, is incomplete. Most commercial alumina materials marketed for their resistance to abrasive and erosive wear have been formulated largely on a trial and error basis, although the beneficial effects of intergranular silicate are well known, and have been the subject of laboratory investigations [4–6]. However, to place the alumina system on a more satisfactory basis relationships between composition, microstructure, wear environment, and wear rate need to be much more clearly defined, and better understood.

Of all the wear processes, erosion caused by impact of hard particles should be the easiest to model, and many studies have been made of both dry and wet erosion (see for example [7, 8]). In the case of dry erosion the angle between the direction of travel of the impacting particle and the surface is an important factor determining wear rate, and can be controlled and readily measured [9]. For wet (slurry) erosion particle impact angles are harder to control and normally but not always [10, 11] an average particle impact velocity has been the parameter used [12]. Because of materials applications in sand blasting and in handling high velocity gas streams containing particulates, in laboratory studies of dry erosion the impact velocities used are normally high ($>10\ \mathrm{m\ s^{-1}}$). In the present study we have explored wet erosion of polycrystalline alumina materials: this is a common industrial wear situation applicable to the pumping and channeling of fluids containing hard particles, and where particle impact velocities are lower. The specific objective has been to obtain

Present Address: Department of Mechanical and Medical Engineering, University of Bradford, Bradford BD7 1DP, UK.

a better understanding of the relationships between the rate of surface degradation of polycrystalline alumina under point impact, and the microstructure of the material expressed in terms of grain size, and secondary phase composition and location.

Surface damage during erosion is initiated by hard particle impact, and in principle it is possible to model the process, and to identify wear mechanisms, by examination of the damage patterns created by single or multiple indentations with a sharp diamond. This was the main method used to characterize materials used in this study. A commonly used model of fracture during wear processes is that based on the radial and lateral crack system surrounding a Vickers indentation [13]. This model has been used with some success to correlate dry erosive wear rates caused by the impact of high velocity (10 to 100 m s^{-1}) particles [7] and the mechanical properties of hardness and fracture toughness. However, the applicability of the model is limited to wear conditions that produce fracture events similar to those produced by the indenter. The Vickers indenter (136% included angle) will not generally produce cracking in a hard ceramic such as alumina at loads below a few Newtons, and once cracking is induced the minimum crack lengths are usually of the order of 10 to 100 μm [14]. This crack pattern may mimic damage caused by the high energy particles in dry erosion processes, but for the slower erosion of alumina by liquidborne particles velocities are of the order of a few m s^{-1}, and this type of test may not be so appropriate. During wet erosion grain fracture is often intergranular, and fracture events produce crack lengths of <10 μm: the associated removal of material then corresponds to the loss of only a few grains at a time. Because the scale of damage caused by a normal Vickers indentation far exceeds this, data obtained from the use of this test does not seem to be well suited as the basis for the construction of a model for wet erosive wear. Indeed, in our work we have found no obvious relationships between hardness and fracture toughness values obtained using the Vickers indenter, and wet erosive wear rates [15]. The simulation of the wet slurry wear environment thus requires experimental techniques capable of producing controlled cracking on a smaller scale than is possible by conventional microhardness testing. A move to a sharper indenter geometry allows cracking to be initiated at lower loads and gives smaller minimum crack lengths, and ideally a conical indenter would be used to remove the artificially imposed fracture directionality of faceted indenters. However, it is difficult (and therefore expensive) to lap a conical diamond indenter to the tip radius of significantly less than the 1 μm required for the type of experiments envisaged here. A reliable and reproducible alternative is the cube corner indenter, which initiates fracture at loads considerably lower than the Vickers, or Berkovich indenters [16], often with loads of less than 100 g.

The detailed study of microcrack initiation at very small loads requires sophisticated testing equipment. One type of experimental system, commonly referred to as nanoindentation, allows the use of loads of a few grammes, giving indentation depths as small as 10 nm, and craters of less than 100 nm in dimension [17]. It also, and most importantly, provides for sensitive continuous recording of load and indentation depth during the indentation loading and unloading cycles. Nanoindentation provides many other advantages over the conventional Vickers of Knoop indentation measurements of hardness and of surface fracture behaviour under loading. Because hardness can be calculated from the indenter displacement, the need to measure the size of the indentation impression is eliminated. The load-displacement trace also records elastic deformation, allowing the calculation of contact stiffness and elastic modulus. Furthermore, specific fracture events are displayed in the load-displacement trace, allowing the load at which crack formation occurs to be identified.

To our knowledge a systematic examination of the mechanical properties and surface fracture behaviour of polycrystalline alumina ceramics using the nanoindentation system has not previously been carried out. This paper reports the results of a preliminary study of the behaviour of a set of alumina materials prepared with magnesium and calcium monosilicate sintering aids, using nanoindentation as the primary method for simulating the response of the materials to the impact of low velocity sharp particles during wet erosion.

2. Experimental

2.1. Materials

Alumina powder (CL3000SG, Alcoa International Ltd. Germany) of stated mean particle dimension 4.2 μm was used both alone (to give pure alumina materials) and with the incorporation of an MO-SiO_2 mixture to provide a liquid sintering aid, where M was the group II metal Mg or Ca. To obtain these blends, alumina powder was mixed with isopropanol solutions of tetraethylorthosilicate (TEOS) ($Si(OC_2H_5)_4$ AnalaR grade, Aldrich, UK) and the hydrated nitrate (AnalaR grade; BDH, UK). Amounts of additives were calculated in order to produce powder containing 10 weight% of equimolar MO-SiO_2. Aqueous ammonium hydroxide was then added to convert the TEOS to hydrated silica and the mixtures were dried at 150°C. Completion of decomposition reactions and dehydration occurred during a subsequent calcination at 900°C for 1 hour. Powders were finally passed through a 100 μm mesh nylon sieve to break up agglomerates.

Discs of material 25 mm in diameter and approximately 6 mm thick were hot-pressed in a cylindrical graphite die at 1450–1600°C and 20 MPa uniaxial pressure. Hot-pressing continued until dilatometry measurements showed a decrease in thickness of 2 μm min^{-1} or less, typically taking 30–60 minutes. Bulk density (ρ) was measured by the water immersion method using BS7134, and porosity was determined by comparing this value to the pycnometry density of a pulverized sample. Mean alumina grain size (G) was calculated from measurements made on scanning electron microscope (SEM) images of polished and thermally etched faces (1450°C for 20 min in air), using a standard line intercept technique [18].

2.2. Indentation procedure

Indentations were carried out on a continuous displacement monitoring indenter (Nanoindenter II, Nano Instruments, Knoxville TN, USA), with a 2 N load head and a cube corner diamond indenter. Indentation samples were cut from hot-pressed discs to give parallel sided sections of approximately 5 mm in thickness. The surface to be indented was lapped to remove cutting damage and then polished to a 1 μm diamond finish. Samples were fixed to aluminium stubs using a hard wax, and the indenter cabinet and sample were allowed to thermally equilibrate for 12 h prior to measurements. The elastic response of the machine (frame compliance) was calibrated using a standard material (vitreous silica). The indenter was loaded at a constant loading rate of 2.5 mN s^{-1} to a peak load of 1300 mN, and unloaded at the same rate to 30% of the peak load, when the load was held for 12.5 s to allow calculation of thermal drift rates; the maximum thermal drift rate was 0.05 nm s^{-1}. Load and corresponding displacement were continuously measured and the data recorded for subsequent processing. This loading procedure was very slow and it took approximately 9 min to achieve the peak value: that is, it corresponded to quasi-static loading. At least 10 indentations were made in each material, spaced at 100 μm intervals. This peak load was thus considerably lower than the minimum load for the fracture of alumina by Vickers indentation which is normally >3N.

2.3. Wear rates

Wear by wet erosion was carried out in a modified high torque attritor mill using 0.5 to 1 mm dimension crushed, fused alumina aggregate in water [19, 20]. The alumina discs were clamped between shaped discs of hard polyurethane attached to the shaft of the mill, with ~50% of the disc exposed. The sample holder was immersed in an externally watercooled slurry consisting of 700 g of alumina grit (of stated purity 92.2% Al_2O_3, with SiO_2 and TiO_2 as the major impurities) in 250 cm^3 of deionised water and rotated at a speed of 8 Hz with a disc track radius of 36 mm (giving a disc perimeter linear velocity of ~1.9 m s^{-1}. A 25 mm gap was left between the lower disc surface, and the bottom of the container to minimize the effects of grit-surface drag. After wearing for 2 hours (t_1) and 6 hours (t_2) discs were ultrasonically cleaned in deionised water, dried for 30 min at 110°C, and weighed to ~100 μg (w_1 and w_2). A wear rate (W_r) (measured in m s^{-1}) was calculated using the expression:

$$W_r = (w_1 - w_2)/\{A\rho(t_2 - t_1)\} \quad (1)$$

where A, arbitrarily, is the area of the exposed leading quadrant of the 6 mm thick disc rim (1/4 of the total rim area or approximately 120 mm^2): experience has shown that with this wear configuration very little wear takes place on the disc faces, and the face area (although much larger) can therefore be ignored. A 4 hour time period was chosen in order to minimize any effects of initial surface finish at short times and the significant smoothing of the grit particles at longer times. The slurry was replaced by a fresh batch after use for two tests (total time 12 hours).

3. Results

3.1. Indentation

Repeated indentation measurements were made on each material. Fig. 1 shows a typical load-displacement trace for an indentation in pure alumina. The reproducibility of the curves was good, with the overall curve patterns matching well and the derived numerical values filling within a band of width ±5% of the mean. The maximum indentation depth (δ_{max}) was typically of the order of 4 μm for indentations obtained under loads of 1 to 2 N used for the cube corner indenter. The shallower three-sided Berkovich indenter gave smaller indentation depths (for the cube corner indenter the projected contact area (A) is given by $A = 24.2\,\delta_{max}^2$: for the Berkovich indenter $A = 4.5\,\delta_{max}^2$). The elastic modulus was calculated using the method of Oliver and Pharr [21], from the slope $S(=dP/d\delta)$ of the upper portion of the unloading curve using the relationship:

$$E_r = S/2(\pi/A)^{1/2} \quad (2)$$

where P is load and δ displacement, and E_r is the reduced modulus given by:

$$1/E_r = (1 - \nu^2)/E + \left(1 - \nu_i^2\right)/E_i \quad (3)$$

E and ν are the Young Modulus and Poisson ratio for the specimen, and E_i and ν_i are the same parameters for the indenter. Hardness (H) was calculated from the projected contact area (A) at the peak load (P_{max}) from the relationship:

$$H = P_{max}/A \quad (4)$$

The maximum plastic displacement (δ_{max}) was taken as the point at which the tangent to the unloading curve at the peak load crossed the displacement axis. Mean values and standard deviations for these parameters are shown in Table I.

The pure alumina was the only material to show discontinuities ("pop-ins" in the load-displacement plots, seen in Fig. 1, during loading. Of the 10 indentations in alumina, 5 showed distinct pop-ins in the loading curve,

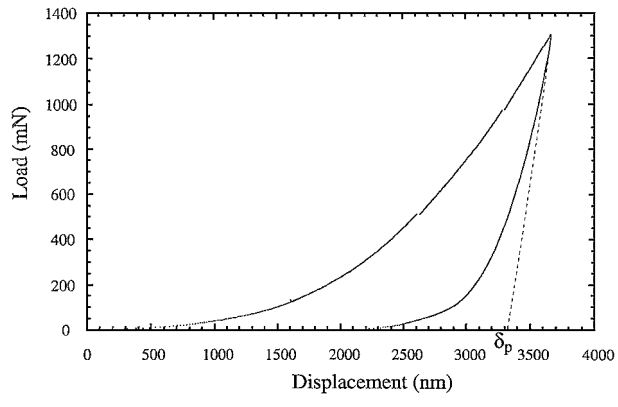

Figure 1 A load-displacement trace typical of an indentation in pure alumina.

TABLE I Mean values and standard deviations for measured data

Material	G/μm	δ_p/nm	δ_{max}/nm	E/GPa	H/GPa	Δe	R_w/nm s^{-1}	Normalized wear rate
Pure Al_2O_3	2.8	3460 ± 270	3950 ± 290	458 ± 75	24.7 ± 3.7	0.124	36.3 ± 0.4	1.08
MgO/SiO_2	2.9	3570 ± 180	4130 ± 210	333 ± 40	23.1 ± 2.2	0.136	11.2 ± 0.9	0.33
CaO/SiO_2	1.9	3500 ± 160	4030 ± 190	379 ± 51	23.8 ± 2.1	0.132	14.0 ± 1.5	0.56

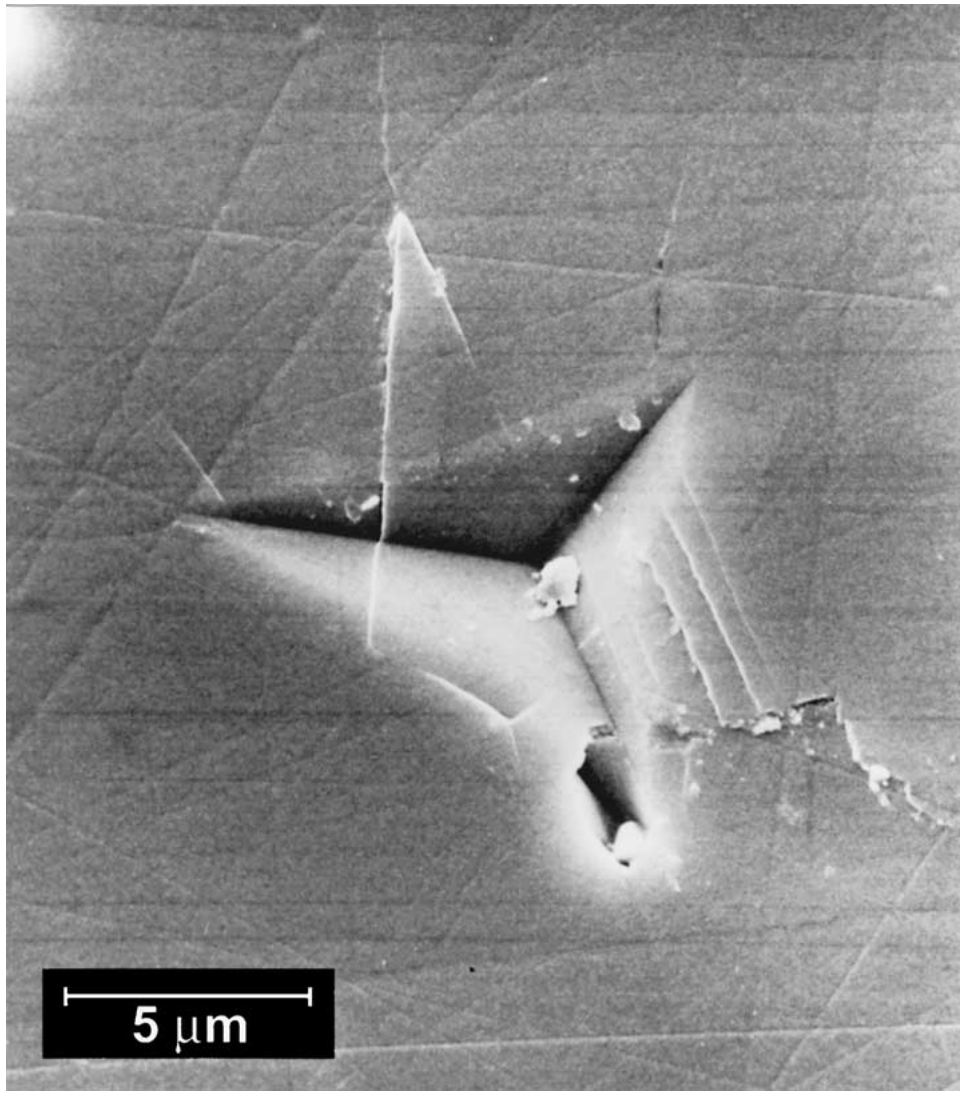

Figure 2 An SEM micrograph of a typical indentation in pure alumina.

while another three showed perturbations in the loading curves of the same order of magnitude as the data sampling resolution. Those indentations where pop-ins occurred generally showed a discontinuity in the displacement of approximately 30 nm between 350 and 750 mN and a second similar sized discontinuity at between 900 and 1150 mN.

3.2. Microscopy

Reflected light microscopy of unetched indented materials showed that the pure alumina materials were extensively microcracked in the vicinity of the indentation: they had radial cracking in 19 of the 20 indentations, and 10 indentations additionally showed one or two lateral cracks. Fig. 2 shows a typical indentation in pure alumina. This shows two large cracks originating in the indentation centre, and the facetted slippage of a grain that the indenter has partially compressed. Fig. 3 is a composite SEM image of the indentation shown in Fig. 2 but now after thermal etching, with a superimposed image of the etched region marked to show the intact grain boundaries in the immediate vicinity of the indentation. Where a crack follows a grain boundary the boundary is not marked: this is the case for the very large grains in the upper part of this picture, which have been partially separated from each other by the crack originating near the central point of the indentation.

The magnesium silicate densified materials were also microcracked. Of ten indentations, seven had associated short radial cracks, which appeared to be transgranular. In addition, two of these indentations showed sub-surface reflection in a semi-circle centred on one of the indentation sides, indicative of

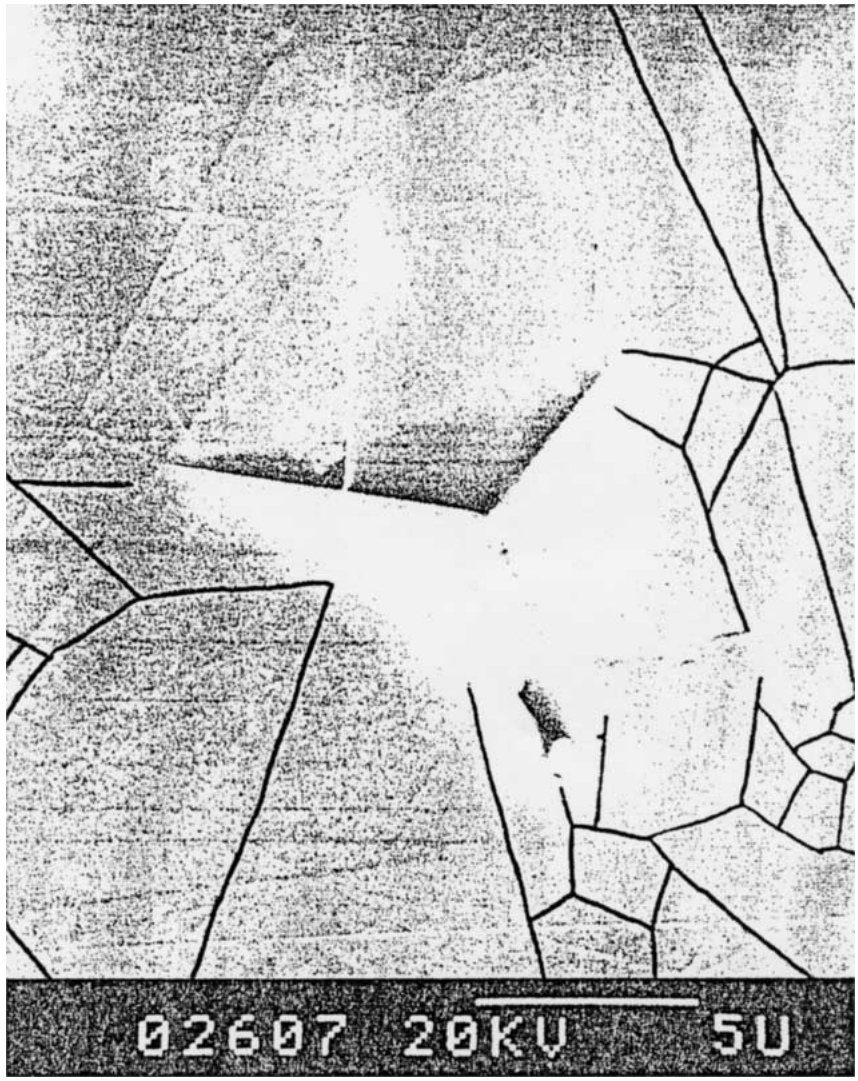

Figure 3 An SEM micrograph of the same indentation, with a superimposed SEM image of the grain boundaries revealed by a thermal etch treatment.

lateral cracking. The calcium silicate densified material showed no cracking or chipping around the indentations.

Mean grain sizes based on the results of line intercept measurements of several hundred grains using SEM micrographs of polished and etched materials, are given in Table I.

3.3. Wear rate

Each disc of material was subjected to two wear tests and the results were averaged. SEM examination of wear surfaces showed that in all cases the predominant wear mechanism was grain boundary microfracture (Fig. 4). The wear rate of alumina in a variety of modes is known to be dependent on grain size [2], and extensive use of the wear test described above has provided a large pool of data for pure aluminas of various grain sizes which has been used to produce an empirical standard curve for the wear rate of pure alumina as a function of grain size. The effect of grain size on the wear rate of an alumina with second phase additions can be allowed for by comparing the wear rate calculated from Equation 1 with the wear rate of a pure alumina of the same grain size. We have called the ratio between these two wear rates the *normalized wear rate*; it is indicative of the degree to which the second phase addition changes the wear rate of the alumina, independent of grain size. Actual and normalized wear data are given in Table 1. For fully dense materials wearing by microfracture the normalized wear rates are reproducible within a factor of $\pm 5\%$.

4. Discussion

4.1. Microstructural aspects

Single crystal aluminium oxide is noncubic (trigonal) and consequently has a marked degree of thermal expansion anisotropy (α), with $\alpha_a = 8.6\ MK^{-1}$ and $\alpha_c = 9.5\ MK^{-1}$ [22]. In polycrystalline alumina materials with randomly oriented and constrained grains, localized thermal expansion mismatch stresses develop on cooling from the processing temperature. The stresses resulting from the anisotropy can be measured using XRD line broadening, and by piezospectroscopy using Cr^{3+} ion fluorescence peak shifts and broadening [23, 24]. Theoretical treatments have shown that the maximum stress in randomly oriented grains of pure polycrystalline alumina should be ~148 MPa, but experimentally much larger (>250 MPa) values have been measured. Because of the greater possibility for

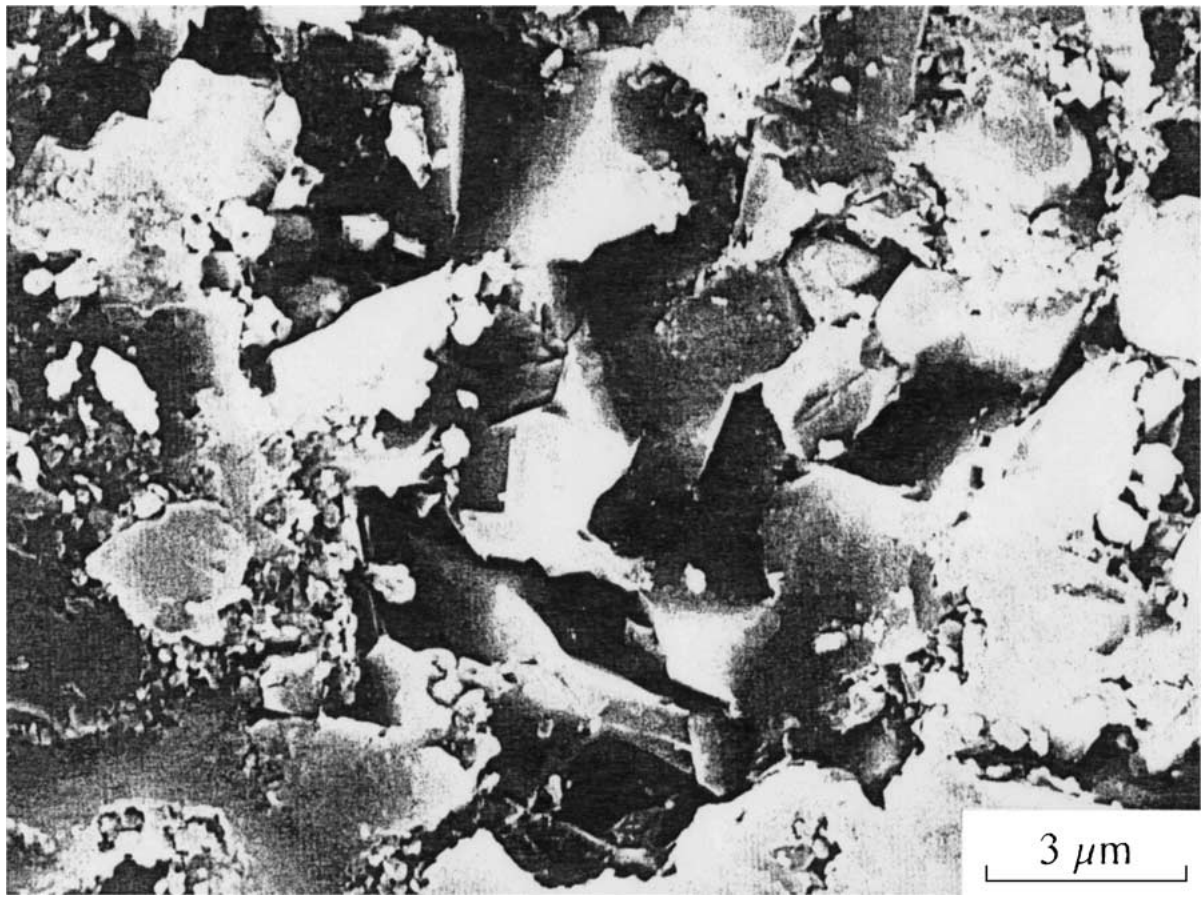

Figure 4 SEM micrograph of a wear surface of pure alumina, showing grain boundary microfracture.

relaxation of the stresses during cooling in materials of smaller grain size, distinct residual stress-grain size relationships are observed, as well as cooling rate - residual stress relationships [25]. Localized thermal expansion mismatch strains have been suggested as being important for the fracture and wear behaviour of sintered alumina [26, 27]. Preliminary measurements on pure polycrystalline alumina, and magnesium silicate densified aluminas of similar grain size have shown that the degree of residual stress is in fact significantly higher in alumina containing magnesium silicate. This is believed to be a consequence of the additional thermal expansion mismatch stresses caused by a low thermal expansivity magnesium aluminosilicate intergranular glass [28].

The Al_2O_3-MgO-SiO_2 system has low melting ternary eutectics at 1345°C and 1360°C and liquid phase sintering of alumina readily occurs in the presence of magnesium silicate. The Al_2O_3-CaO-SiO_2 system has a set of lower melting point eutectics (the lowest at 1170°C) that facilitate even faster liquid phase sintering [29, 30]. Because of the effectiveness of the calcium silicate sintering aid system, a shorter hot-pressing time is required for full density to be reached and therefore there is less time for grain growth to occur; the resulting materials had a small mean grain size (smaller in fact than the alumina powder apparent average particle size, indicating that the primary particles are agglomerated). Longer densification times were required for the magnesium silicate densified alumina, and for pure alumina, and the mean grain sizes were correspondingly larger.

The magnesium and calcium silicates used here both produced almost entirely glassy intergranular phases, as far as could be judged from XRD examinations. Earlier studies using a scanning electron microscope with an EDX analysis facility had shown that silicates may in part form intergranular magnesium aluminate spinel, or calcium hexaluminate, as expected from the phase equilibrium diagrams [30]. Detailed examinations of calcium silicate densified alumina by high resolution analytical TEM/STEM (using EDX and EELS) show that most if not all of the very thin two-grain boundaries contain an amorphous calcium aluminosilicate phase of compositions intrinsically linked to, but not necessarily always the same as that of the overall system composition [31, 32]. The thickness of the two-grain boundaries varies with the CaO/SiO_2 and is of the order of 0.8 to 2.0 nm, which may be explained in terms of a Force Balance model [33]. It has been suggested that the differences in glass chemistry at the two grain faces are in part directly responsible for observed differences in erosive wear rate.

4.2. Indentation behaviour

The influence of additive system on the behaviour of the aluminas was seen in comparisons of their responses to indentation, and the extents of indentation crack development. For all materials the curves for displacement as a function of load showed the characteristic hysteresis loop to be expected from a material having a combination of elastic and plastic response to the

indenter (Fig. 1). The pure alumina material showed the expected correlation between the production of pop-ins during loading and the appearance of extensive networks of microcracks around the indentations. Pop-ins were only detected in the loading curves, which indicated that the associated fracture events occurred during this stage of the cycle. Other studies have provided direct evidence for the onset of different types of cracking during loading and unloading by microscopic observation under load [34]. However, this direct observation is only possible in transparent materials and so excludes most polycrystalline ceramics. Although the alumina densified with magnesium silicate showed microcracking in about 70% of the indentations, surprisingly there were no pop-ins. It is not yet clear why these fracture events were not revealed in the load-displacement curve.

The area under the displacement as a function of load curve is a measure of the work of indentation: the area under a pop-in provides an estimate of the energy associated with that event. As a typical example, one indentation showed a pop-in from 3010 nm to 3040 nm at a load of 712 mN: the associated energy is 21 nJ. All of the observed pop-in events had associated energies of between 10 and 35 nJ. Assuming for alumina a single crystal fracture surface energy of 6 J m^2 (for the 1102 face [35]), 21 nJ is able to generate 3500 μm^2 of fracture surface. This energy would be capable of generating a smooth semicircular crack of diameter 67 μm. The cracks observed in the alumina were of the order of 5 μm in length and the pop-in events are clearly able to provide more than sufficient energy for the generation of a local surface crack system. As can be seen from Fig. 2, the cracks correspond to a roughly equal mixture of inter and intra-granular fracture, from which it is deduced that the inter- and intragranular fracture energies are similar in magnitude.

The degree of elastic recovery (Δe) on unloading the indenter can readily be calculated from:

$$\Delta e = (\delta_{max} - \delta_p)/\delta_{max} \quad (5)$$

where δ_{max} is the maximum displacement and δ_p the residual plastic displacement after unloading. Experimentally determined values for the degree of elastic recovery (which, because it is measured with reference to maximum displacement of the diamond is not strictly a strain) are about 0.124 for the pure alumina, 0.136 for the calcium silicate densified material, and 0.132 for the magnesium silicate.

For metals, the capacity for purely elastic deformation is indicated by the yield strain, which is defined as the elastic strain at the point on loading in a tensile test when plastic flow starts to occur [36]. However, indentation loading does not correspond precisely to a tensile test, in that irreversible plastic deformation of the material at the indenter tip, and local elastic displacement of the surface under the load transmitted by the indenter, occur simultaneously. The total extent of plastic deformation is moreover likely to be the sum of a plastic deformation component, and a component associated with crack development in the region of the indentation.

The mean value of E (458 GPa) for polished pure polycrystalline alumina determined from the initial slope of the unloading curve is in close agreement with the generally accepted maximum literature value for single crystal alumina of about 460 GPa, for the ⟨0001⟩ direction [37]. Using a Berkovich indenter, Cook and Pharr [34] measured 441 GPa for 001 single crystal sapphire, a value significantly higher than the Voigt/Reuss average of 403 GPa, possibly because of the dominant influence of the large c-axis modulus (assumed in this paper to be 499 GPa [38]). The value determined in the present study is the mean of 10 indentations, and thus the average value for many crystal orientations. The slightly high value (by about 15%) compared with those previously reported may be the result of an error in the diamond tip area calibration. However, a similar unexpectedly high value of E for 001 single crystal quartz was measured by Oliver and Pharr, where the measured modulus of 124 GPa was higher than both the Voigt/Reuss average of 95 GPa and the c-axis modulus of 105 GPa. In contrast, for materials with isotropic elastic properties good agreement was obtained between measured and literature moduli. Although nominally uniaxial, creation of the indentation involves deformation in many directions; It might therefore be expected that for anisotropic materials some averaged value of modulus would be recorded. The influence of elastic anisotropy on this type of measurement using indentation load-displacement methods clearly requires further study. However, in the present context of the evaluation of the mechanical properties of members of a set of related polycrystalline materials, the absolute values of the moduli are likely to be less important than differences between them.

The addition of 10% magnesium silicate and calcium silicate reduced the modulus significantly (by 27 and 17% respectively). The presence of an intergranular glass of low modulus in the polycrystalline alumina would be expected to reduce E [38]. The experimentally measured value for a 90% commercial alumina is about 300 GPa: a calculation assuming a second phase containing 33% Al_2O_3 of density 2.7 Mg m^{-3}, and moduls 100 GPa suggests a higher value of around 390 GPa [3]. There is no indication that alumina materials containing different types of silicate should have different overall moduli, provided these general assumptions are met. While the measured value for the calcium silicate material approaches the calculated estimate, that for the magnesium silicate is much lower, and there is no immediate explanation.

It would be expected that for the silicate-containing aluminas, with pockets of amorphous material at the grain edges ("triple points") and of overall volume ~10 to 20%, some indentations would penetrate preferentially the silicate, others entirely an alumina grain. However, the spreads of modulus values for all indentations, irrespective of the material, were similar, and if anything slightly higher for the pure alumina (±16% compared with ±12%). The likely explanation is that with the 1 to 2 N loads used giving maximum displacements of ~4 μm, the indenter is in all cases able to penetrate the small glass pockets into the underlying

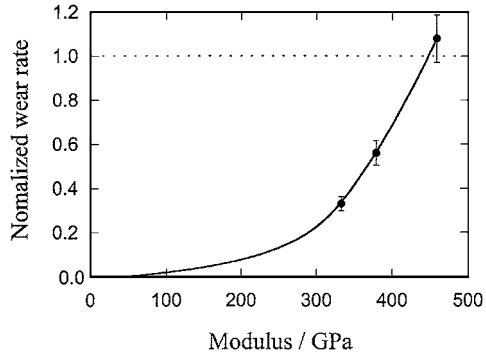

Figure 5 Wear rate as a function of low load modulus.

alumina grains, and is therefore detecting the response of the whole microstructure. The indentation load distributed over the indentation is still too large, and several phases are covered: for possible differences between these materials to be detectable, moduli would need to be measured using much smaller maximum loads.

In marked contrast, the presence of the silicates had no significant effect on the residual plastic component of deformation from which hardness was calculated; the hardnesses of the three materials were within experimental error identical.

The differences in degree of elastic recovery were small, though the two silicate containing aluminas had slightly higher values. The high values of Δe would indicate ability to accommodate local stresses caused by a single impact, without extensive microcracking or other form of permanent damage. The liquid phase sintered aluminas therefore appear not only to be less stiff, but also more readily to store strain energy, until a level is reached at which crack initiation can occur. There is speculation regarding the physical origin of the pop-in event in the polycrystalline alumina materials. At the load corresponding to the appearance of the pop-in, the indenter diamond is just supported by the stressed surrounding material. The sudden development of a cracking around the diamond allows local relaxation of the material, with partial release of strain. Small abrupt increases in penetration depth at constant load would then be caused by the momentary decrease in contact area between the diamond tip and the contacting material (which is supporting the constant downwards force applied electromagnetically to the diamond). Consequently the downwards stress (force/area) momentarily increases, resulting in an associated displacement of the material by the diamond, until the supporting contact area again matches that required by the downwards load.

4.3. Wear

The normalized data show that both magnesium and calcium silicate additives significantly reduce the alumina wear rate (for similar grain size materials), with magnesium silicate being the most effective. On the basis of the evidence provided by the nanoindentation measurements and observations of surface damage, a mechanism is suggested giving the silicate densified aluminas an increased resistance to loss of material. The intergranular silicates appear to provide both materials with greater resilience under point loading, the magnesium silicate being particularly effective. Because of the apparent influence of composition on Δe, coupled with an insensitivity of hardness to composition, it might be expected that Δe would be primarily influenced by modulus. A plot of wear rate expressed as a function of low load modulus is a smooth curve (Fig. 5), provided support for the view that local elastic behaviour is a major factor controlling wet erosive wear rates.

The more qualitative aspects of the nanoindentation, the degree of microcracking generated and the pop-in frequency, are not entirely consistent with the quantitative measurements of wear rate. While the pure alumina is clearly lacking tolerance to loading, the differences between the silicate densified materials are not easy to explain, and further work is called for. The differences in extent of cracking between the pure alumina and the two liquid phase densified materials would be consistent with grain boundary strengthening in the silicate materials, causing inhibition of grain boundary crack propagation. Computer modeling of microstructures and properties of grain boundaries in alumina containing silica and magnesium oxide, shows the beneficial influence of magnesium silicate on grain boundary strength [39]. The evidence for continuous amorphous films at two-grain boundaries in calcium silicate densified alumina has been referred to above, but similar examinations of magnesium silicate containing materials appear not to have been carried out. On the basis of calculated thermal expansion coefficient differences between alumina and silica-rich grain boundary aluminosilicate glasses, compressive grain boundary hoop stresses would be expected for a magnesium silicate densified material, in which the continuous phase is a silicate glass.

5. Conclusions

The nanoindentation technique allows surface damage events on the scale of a few μm to be studied, and a semiquantitative evaluation of a set of related materials to be obtained. The addition of silicate sintering additives to alumina produces marked changes in response to the indenter under loads of a the order of 50 to 100 g. Pure alumina, with high stiffness and hardness, has a relatively low resistance to microcrack initation and damage. Correlations with wear rate are obtained with local low load modulus. Alumina densified with liquid phase sintering aids has closely similar hardness but significantly lower modulus. The liquid phase sintered materials have a greater resistance to microcracking at these loads, and a lower wear rate. The reason for the beneficial action of silicates is postulated to be a combination of two factors: the introduction of compliant intergranular films of low effective modulus providing protection against microcrack initiation, and an increase in bond strength between atoms forming two-grain boundary films through reduction in the excess energy caused by bond misalignment.

Acknowledgements

The programme was funded by EPSRC Research Grant GR/J86513. Prof. J. Pethica and Dr. S. Asif of the

University of Oxford Department of Materials are thanked for their advice and guidance with nanoindenter measurements. Alcoa International Ltd. is thanked for the supplies of alumina powder.

References

1. I. M. HUTCHINGS, *J. Physics D: Applied Physics* **25** (1992) A212.
2. R. W. DAVIDGE and F. L. RILEY, *Wear* **186/187** (1995) 45.
3. R. MORRELL, "Handbook of Properties of Technical & Engineering Ceramics: 2. Data Reviews, Section I: High-Alumina Ceramics" (HMSO, London, 1987).
4. P. C. TWIGG, R. W. DAVIDGE, S. G. ROBERTS and F. L. RILEY, in Euro Ceramics V, edited by J. Baxter, L. Cot, R. Fordham, V. Gabsis, Y. Hellot, M. Lefebvre, H. LeDousal, A. LeSech, R. Naslain and A. Sevagen, *Key Engineering Materials* **132–136** (1997) p. 1524.
5. C. P. DOGAN and J. A. HAWK, *Wear* **181**(1) (1995) 129.
6. J. R. ZHOU and S. BAHADUR, *ibid.* **162**(A) (1993) 285.
7. P. H. SHIPWAY and I. M. HUTCHINGS, *ibid.* **193**(1) (1996) 105.
8. S. LATHABAI, *Materials Science Forum* **19** (1995) 101.
9. Y. I. OKA, H. OHNOGI, T. HOSOKAWA and M. MATSUMARA, *Wear* **203** (1997) 573.
10. A. FRANCO and S. G. ROBERTS, *J. European Ceram. Soc.* **18**(3) (1998) 269.
11. Y. XIE, C. M. CLARK and H. M. HAWTHORNE, *Wear* **229**(1) (1999) 405.
12. M. M. STACK and N. PUNGWIWAT, *ibid.* **215**(1/2) (1998) 76.
13. D. B. MARSHALL, B. R. LAWN and A. G. EVANS, *J. Amer. Ceram. Soc.* **65**(10) (1982) 561.
14. J. LANKFORD and D. L. DAVIDSON, *J. Mater. Sci.* **14** (1979) 1662.
15. D. GALUSEK, P. C. TWIGG and F. L. RILEY, *Wear* **233–235** (1999) 588.
16. G. M. PHARR, D. S. HARDING and W. C. OLIVER, in NATO ASI Series E: Applied Sciences Vol. 223, edited by M. Nastasi, D. M. Parkin and H. Gleiter (Kluwer Academic Publishers, Boston, 1993).
17. T. F. PAGE, in Proc. First Royal Society-Unilever Indo-UK Forum in Materials Science and Engineering, edited by M. J. Adams, S. K. Biswas and B. J. Briscoe (Imperial College Press, London, 1996) p. 93.
18. M. I. MENDELSON, *J. Amer. Ceram. Soc.* **52** (1969) 443.
19. M. MIRANDA-MARTINEZ and F. L. RILEY, *Brit. Ceram. Trans. & J.* **90**(4) (1991) 118.
20. M. MIRANDA-MARTINEZ, R. W. DAVIDGE and F. L. RILEY, *Wear* **172** (1994) 41.
21. W. C. OLIVER and G. M. PHARR, *J. Mater. Res.* **7**(6) (1992) 1564.
22. R. W. RICE and S. W. FREIMAN, *J. Amer. Ceram. Soc.* **64**(6) (1981) 350.
23. A. KRELL, A. TERESIAK and D. SCHLAFER, *J. Eur. Ceram. Soc.* **16** (1996) 803.
24. Q. MA and D. R. CLARKE, *J. Amer. Ceram. Soc.* **77**(2) (1994) 298.
25. J. E. BLENDELL and R. L. COBLE, *ibid.* **65**(3) (1982) 174.
26. R. W. RICE and R. C. POHARKA, *ibid.* **62** (1979) 559.
27. A. K. MUKHOPADHYAY and Y.-W. MAI, *Wear* **162–164** (1993) 258.
28. D. GALUSEK, F. L. RILEY, A. ATKINSON, Y. ZHANG and R. BRYDSON, *Key Engineering Materials* **175/176** (1999) 189.
29. E. M. LEVIN, C. R. ROBINS and H. F. MCMURDIE (eds.), "Phase Diagrams for Ceramists" (The American Ceramic Society, Columbus, Ohio, 1964) Figs 630 and 712.
30. O. ABDUL KADER, Ph D thesis, University of Leeds, 1993.
31. R. BRYDSON, P. C. TWIGG, S. C. CHEN, F. L. RILEY, X. PAN and M. RÜHLE, *J. Amer. Ceram. Soc.* **81**(2) (1998) 369.
32. R. BRYDSON, P. C. TWIGG and F. L. RILEY, *J. Mater. Res.* **81**(3) (2001) 369.
33. D. R. CLARKE, *J. Amer. Ceram. Soc.* **70**(1) (1987) 15.
34. R. F. COOK and G. M. PHARR, *ibid.* **73**(4) (1990) 787.
35. S. M. WIEDERHORN, *ibid.* **57** (1969) 485.
36. D. TABOR, *Proc. Royal Soc. A* **192** (1948) 247.
37. J. B. WACHTMAN, W. E. TEFFT, D. G. LAM and R. STINCHFIELD, *J. Res. Nat. Bur. Stds* **64A** (1960) 213.
38. G. SIMMONS and H. WANG, "Single Crystal Elastic Constants and Calculated Aggregate Properties: A Handbook," 2nd ed. (The MIT Press, Cambridge, MA, 1971).
39. S. BLONSK and S. H. GAROFALINI, *J. Amer. Ceram. Soc.* **80**(8) (1997) 1997.

Received 12 April 2000
and accepted 28 August 2001